INTERNATIONAL JOURNAL OF PRECISION ENGINEERING AND MANUFACTURING Vol. 18, No. 4, pp. 471-478 APRIL 2017 / 471

REGULAR PAPER

DOI: 10.1007/s12541-017-0057-9
ISSN 2234-7593 (Print) / 2005-4602 (Online)

An Active Radial Compliance Method with Anisotropic Stiffness Learning for Precision Assembly

Fang-Bo Qin[1,2], De Xu[1,2], Deng-Peng Xing[1,2,#], and Zheng-Tao Zhang[1,2]

1 Research Center of Precision Sensing and Control, Institute of Automation, Chinese Academy of Sciences, Beijing, 100190, China
2 School of Computer and Control Engineering, University of Chinese Academy of Sciences, Beijing, 101408, China
Corresponding Author / E-mail: dengpeng.xing@ia.ac.cn, TEL: +86-10-82544760-813, FAX: +86-10-82544760-806

KEYWORDS: Active compliance, Force control, Learning from experience, Vision measurement, Precision assembly

Compliance is essential for precision assembly, which provides motion guidance and damage avoidance. Force control can offer flexible implementation of active compliance for manipulators. In this paper, an active radial compliance method is developed for the insertion task of thin walled millimeter-sized cylinders. A radial force controller is designed to satisfy the contact force constraint in the component's radial directions, which integrates the explicit force control with the high precision attitude measurement based on microscopic vision. An anisotropic stiffness learning method is proposed based on clustering and support vector machines. It can obtain the hidden anisotropic stiffness characteristics of the mechanical system from experience data. Experimental results verify the effectiveness of the proposed methods.

Manuscript received: June 4, 2016 / Revised: October 31, 2016 / Accepted: December 7, 2016

NOMENCLATURE

$\boldsymbol{v}_a$ = attitude of component's axis
$\boldsymbol{J}$ = image Jacobian matrix
$\boldsymbol{l}$ = vector in the image
$\boldsymbol{f}_r$ = contact force in component's radial direction
$\boldsymbol{f}_d$ = desired contact force in component's radial direction
$\boldsymbol{e}_f$ = contact force error in component's radial direction
λ = controller gain
τ = dead zone threshold of controller
h = insertion depth
$\tilde{k}_i$ = estimated stiffness of a sample
k_+, k_- = high and low stiffness in different directions
C_+, C_- = classes with high and low stiffness
H, H_A, H_{I+}, H_{I-} = insertion depth region and its subregions
$\boldsymbol{w}$, b = normal vector and offset of separating plane in SVM
$\tilde{r}$ = geometric margin in SVM
c = penalty parameter in SVM
d_+, d_- = parameters determining boundary of fuzzy region

1. Introduction

Manipulator compliance plays an essential role in assembly tasks. In many cases, manipulator's end pose is constrained by environment, so that compliance is required to provide position compensation and protection against contact damage. Active compliance fulfilled by force control has advantages over passive compliance provided by external tools in the flexibility to regulate and the simplicity to design.[1] The explicit force control[2,3] and impedance control[4] are two main approaches in force control. Other enhanced methods such as hybrid position/force control[5,6] and adaptive control[7] are based on these two methods. Explicit force control is more suitable for the application of maintaining a desired contact force.

Precision assembly manipulating the components with micrometers- or millimeters-level sizes has been drawing more and more attention.[8-11] The tolerable contact force in precision assembly task is much smaller than that in conventional assembly. Generally, both force and position feedbacks are integrated into the designed controller. For example, Xu proposed a simultaneous position/force tracking control method for a piezoelectric microgripper dedicated to microassembly tasks.[12] Komati et al. achieved the compliant guidance of a flexible micropart to pass along a rail using hybrid position/force control. The lateral contact force was maintained at a few of tens μN.[13] However, these 1-demensional

force control methods are not adequate for assembly in 3-Demensional (3D) space. In the insertion task, the component's position is adjusted to reduce the contact forces between the two assembled components according to force feedbacks. For example, a high precision automatic assembly system in 3D space was developed, which aligns the components based on microscopic vision and inserts the lower component into the upper one based on force information.[14] However, the total insertion depth was only 800 μm. In many cases, the insertion depth is several millimeters, and the increment of contact area might pose more difficulty to compliant insertion. Xing et al. proposed a coordinated insertion control strategy for inclined precision assembly, which contained the active compensational motion for the inclined posture and deviated insertion direction and the passive compensation based on the force-feedback.[15] The horizontal contact force was constrained within 150 mN. However, the coordinated insertion method highly relies on the precise kinematic model and exact pose feedback of coordinating manipulator.

In automation and robotics areas, learning algorithms offer new opportunities to improve the system's performance. An impedance learning method was proposed to adjust the impedance parameters of the robot arm iteratively subject to unknown environments, which employed the gradient-following scheme and betterment scheme.[16] An unsupervised learning algorithm based on logic branching trees was developed to generate condition-action rules for automated inserting assembly.[17] Li et al. proposed a supervised learning assisted reinforcement learning method for the path planning in microassembly.[18] It is very helpful to employ the learning methods to obtain the object's or the assembly system's characteristics and improve the system's performance. The application of learning algorithm in precision assembly domain remains to be explored.

The motivation of this work is to deal with the hidden anisotropic stiffness characteristic of precision assembly and consequently propose an active compliance method for insertion. This paper mainly focuses on two problems: 1) the insertion of thin-walled objects with interference fit, which requires high precision of force control; 2) stiffness anisotropy that may exist in some precision assembly platform. To address these problems, we present an anisotropic stiffness learning method based on clustering and support vector machines to obtain the hidden anisotropic stiffness characteristics from experience data. An anisotropic stiffness radial force control strategy is developed to adjust the contact force in the component's radial directions. Comparative experiments with the proposed controller and the traditional controller are conducted to evaluate their performances under different component attitudes.

The rest of this paper is organized as follows. In Section 2, the system configuration and task specification are introduced. In Section 3, an anisotropic stiffness radial force control method is designed. The learning method of anisotropic stiffness characteristics is proposed in Section 4 Section 5 presents the experiments and results. Finally, it is concluded in Section 6.

2. System Design and Task Specification

The assembly system is designed as given in Fig. 1. It consists of two manipulators, two microscopic cameras, a force sensor and a manual regulation stage. The components to be assembled are a cylinder and a sleeve. The cylinder is gripped on the top center of the end of manipulator B with two translational DOFs and three rotational DOFs. The sleeve is held by a vacuum gripper at the end of manipulator A with 3 translational DOFs. The manual regulation stage owns three rotational DOFs to adjust the sleeve's attitude manually at the beginning of assembly cycles. The components' poses in 3D space are measured by the two microscopic cameras. The force sensor is fixed at the wrist of manipulator A to measure 6-Demensional (6D) force and torque.

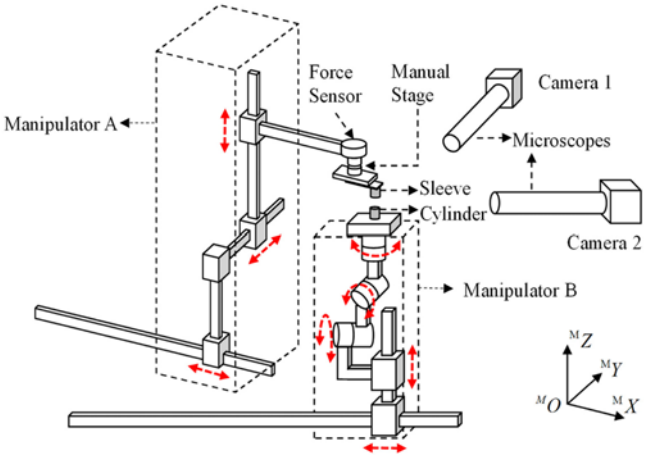

Fig. 1 System configuration sketch

The assembly task is to insert the cylinder into the sleeve. The whole assembly process includes the alignment phase and the insertion phase. In the alignment phase, an image-based PI controller generates the aligning motions according to the visual feedbacks.[14] The manipulator B aligns the cylinder's attitude to the sleeve's, and then the manipulator A aligns the sleeve's position to the cylinder's. In the insertion phase, the visual feedbacks become unavailable due to the sight blocking, and the force feedbacks are essential to compensate for position errors and protect the components. As the cylinder is inserted upward gradually, the manipulator A provides compliant motions of the sleeve. The cylinder is vulnerable to contact force that is perpendicular to the component surface. The two components for assembly have an interference fit between each other, i.e., the inner component's radius is no smaller than the outer one's and a pushing force is required for insertion.

3. Radial Force Control

Since only the contact force constraint in the components' radial directions is required and the components' attitudes might be slightly inclined in the force sensor coordinates, the measured force is decomposed into the radial contact force and the axial pushing force, based on the attitude measurement given by the vision system. The radial contact force is used as the feedback in the radial force controller to ensure the radial contact force under desired value. In addition, the contact directions and insertion depth are considered as factors that determine the contact stiffness.

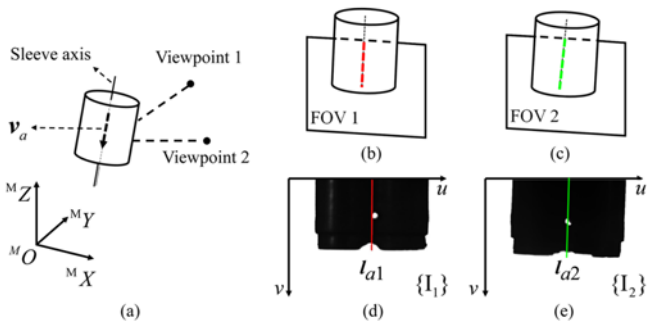

Fig. 2 Vision measurement of the sleeve axis's attitude, (a) sleeve and two cameras' viewpoints in the manipulator coordinates {M}, (b) field of view of camera 1, (c) field of view of camera 2, (d) image in camera 1, (e) image in camera 2

3.1 Attitude measurement based on microscopic vision

The sleeve axis's attitude $\boldsymbol{v}_a \in \mathbb{R}^{3\times1}$ in the manipulator coordinates {M} is measured by the two microscopic cameras, as shown in Fig. 2. The image coordinates of the cameras 1 and 2 are labeled as $\{I_1\}$ and $\{I_2\}$, respectively. The image Jacobian matrix $\boldsymbol{J} \in \mathbb{R}^{2\times3}$ maps a 3D vector $\boldsymbol{v} = [\Delta x, \Delta y, \Delta z]^T$ in {M} into the image space as an vector $\boldsymbol{l} = [\Delta u, \Delta v]^T$, i.e., $\boldsymbol{l} = \boldsymbol{J}\boldsymbol{v}$. Δu and Δv are the position changes along the u-axis and v-axis of the image coordinates, respectively. Using the two cameras 1 and 2, we have

$$\begin{cases} \boldsymbol{l}_{a1} = \rho_1 \boldsymbol{J}_1 \boldsymbol{v}_a \\ \boldsymbol{l}_{a2} = \rho_2 \boldsymbol{J}_2 \boldsymbol{v}_a \end{cases} \tag{1}$$

where $\boldsymbol{l}_{a1}$ and $\boldsymbol{l}_{a2}$ are the sleeve axis's image vectors in $\{I_1\}$ and $\{I_2\}$, respectively. ρ_1 and ρ_2 are the scaling factors indicating the axial line segments' lengths. $\boldsymbol{J}_1$ and $\boldsymbol{J}_2$ are the image Jacobian matrices associated with the cameras 1 and 2, respectively.

To obtain the sleeve axis's image vectors, the image processing techniques are applied. Firstly, the sleeve is recognized and segmented with the template matching method. Then the Canny algorithm is employed to detect the edges on the component's contour. The edges and line fitting method are used to figure out the equations of the sleeve image's sides. The midline of the left and right sides is the projection of the sleeve axis, and this midline's direction vector is $\boldsymbol{l}_{ai} = [\Delta u_i, \Delta v_i]^T$ (i = 1, 2). Let $\boldsymbol{l}_{pi} = [-\Delta v_i, \Delta u_i]^T$ denote the perpendicular vector of $\boldsymbol{l}_{ai}$, so that $\boldsymbol{l}_{pi}^T \boldsymbol{l}_{ai} = \boldsymbol{l}_{pi}^T \boldsymbol{J}_i \boldsymbol{v}_a = 0$. Eq. (1) can be rewritten as a homogeneous equation,

$$\boldsymbol{U}\boldsymbol{v}_a = \begin{bmatrix} \boldsymbol{l}_{p1}^T \boldsymbol{J}_1 \\ \boldsymbol{l}_{p2}^T \boldsymbol{J}_2 \end{bmatrix} \boldsymbol{v}_a = \boldsymbol{0} \tag{2}$$

where $\|\boldsymbol{v}_a\| = 1$. The estimation of $\boldsymbol{v}_a$ can be solved by using the optimization

$$\min_{\boldsymbol{v}_a} \left\| \boldsymbol{U}\boldsymbol{v}_a \right\|^2, \ \text{s.t.} \ \left\| \boldsymbol{v}_a \right\| = 1 \tag{3}$$

The optimal solution of $\boldsymbol{v}_a$ is given by the eigenvector $\boldsymbol{e}$ associated with the minimum eigenvalue of $\boldsymbol{U}^T\boldsymbol{U}$.[19]

3.2 Anisotropic stiffness radial force control system

To achieve the active compliance at the manipulator's end, the control system with an explicit force controller based on the inner position loop is designed, as shown in Fig. 3. In the inner position loop, the manipulator controller P_m executes the incremental motion $\Delta\boldsymbol{x}$ given by the outer force loop. The position error $\boldsymbol{e}_x$ between the sleeve's radial position $\boldsymbol{x}_m$ and the cylinder's radial position $\boldsymbol{x}_h$ causes the radial contact force $\boldsymbol{f}_r$. The axial pushing force $\boldsymbol{f}_a$ is generated to overcome the friction due to the interference between components. In the force sensor module S_f, the force sensor's output $\boldsymbol{f}$ is filtered by a Butterworth low-pass filter and is transformed from the sensor coordinates {S} to the manipulator coordinates {M}. Then the force decomposer D_f gives the radial contact force $\boldsymbol{f}_r$ according to the sleeve axis's attitude $\boldsymbol{v}_a$ that is measured by vision system.

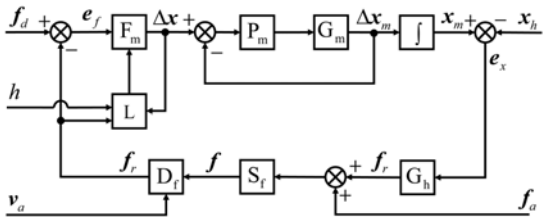

Fig. 3 Block diagram of the anisotropic radial force control system. F_m: Incremental controller. P_m: Position controller. G_m: Manipulator. $\int$: Integrator. G_h: Radial contact model. S_f: Force sensor module. D_f: Force decomposer. L: Anisotropic stiffness learning module

$$\boldsymbol{f}_r = \boldsymbol{f} - (\boldsymbol{v}_a \cdot \boldsymbol{f})\boldsymbol{v}_a \tag{4}$$

In the outer force loop, the manipulator's incremental motion is formed by the incremental controller F_m. Its control law is designed as

$$\Delta\boldsymbol{x}(t) = \begin{cases} 0, & \| \boldsymbol{e}_f(t) \| < \tau \\ -\lambda \boldsymbol{e}_f(t), & \| \boldsymbol{e}_f(t) \| \geq \tau \end{cases} \tag{5}$$

where λ is the gain factor. $\boldsymbol{e}_f(t)$ is the error between the desired and measured radial forces. A dead zone [0, τ) is used to avoid frequent adjustment, so that F_m produces nonzero output only when the error's magnitude is larger than τ. The desired contact force $\boldsymbol{f}_d$ is kept as zero for the compliance purpose.

In the anisotropic stiffness force control system, the learning module L learns the anisotropic stiffness characteristics from experience data, and identifies the current stiffness according to the current radial contact force $\boldsymbol{f}_r$ and the current insertion depth h. Then F_m adjusts its gain factor by

$$\lambda(t) = 1/K[\boldsymbol{f}_r(t), h(t)] \tag{6}$$

where $K(\boldsymbol{f}_r, h)$ is the stiffness given by L.

4. Anisotropic Stiffness Learning

Stiffness anisotropy means that the stiffness is dependent on contact direction, as opposed to *stiffness isotropy* that implies an identical stiffness in all directions. The main reason for stiffness anisotropy is the asymmetric mechanical structure.

As the contact force is dependent on the contact direction, there exists a relationship from the current contact force $\boldsymbol{f}_r$ to the stiffness. The stiffness anisotropy can be extracted from the experience data of past assembly processes. Considering that the insertion depth might affect the stiffness, the insertion depth h is involved in stiffness identification. Therefore, we design the anisotropic stiffness learning method, which includes three steps: samples collection, clustering, and classification.

4.1 Samples collection

Since the radial force control with a constant gain can maintain the radial contact force within the non-damage range, the past assembly cycles are conducted based on this control method. Each time the compliant motion begins, we record the initial radial contact force $\boldsymbol{f}_{ri}$, the current insertion depth h_i, and the estimated stiffness $\tilde{k}_i$ given by

$$\tilde{k}_i = \|\Delta \boldsymbol{f}_{ri}\| / \|\Delta \boldsymbol{x}_i\| \tag{7}$$

where $\Delta \boldsymbol{f}_{ri}$ is the variation of radial contact force caused by the sleeve's compliant motion $\Delta \boldsymbol{x}_i$. After several times of assembly, an sample set $\{\tilde{k}_i, \boldsymbol{f}_{ri}, h_i\}$ (i = 1, 2, …, N) is obtained, using which the relationship between stiffness, contact direction, and insertion depth can be analyzed.

4.2 Clustering

Clustering, which can find the implicit classes in samples set based on degree of similarity, is used to determine whether multi classes with different stiffness exist. If the stiffness is anisotropic, the samples will be grouped into different clusters. The samples in the same cluster own similar stiffness, and the samples in different clusters own distinct stiffness. DBSCAN (Density-Based Spatial Clustering of Applications with Noise) algorithm is utilized to find the clusters.[20] DBSCAN relies on a density based notion of clusters and is able to discover noise as well. Its key idea is that for each sample points in a cluster the neighborhood of a given radius Eps has to contain at least a minimum number of points (MinPts), and the points belonging to none of the clusters are considered as noise. The stiffness is used to measure the distance between samples, as given by

$$dist(i,j) = |\tilde{k}_i - \tilde{k}_j| \tag{8}$$

If two or more clusters are discovered, the classification procedure is needed. If there exists only one cluster, the stiffness is considered isotropic and the classification procedure is not necessary.

4.3 Classification

For a new data sample during a new insertion, the current status $\{\boldsymbol{f}_r, h\}$ is known before adjustment, and the current contact stiffness is predicted by identifying which class it belongs to. The identifying model is trained by experience data. For a two-class classification, the samples in the class C_+ have the high stiffness k_+, and the samples in the class C_- have the low stiffness k_-.

The insertion depth region H is divided into the sub-regions H_{I+} with high stiffness, H_{I-} with low stiffness and H_A with anisotropic stiffness according to the data samples' distribution in H. Let H_+ denote the sub-region where the insertion depths of all the high stiffness samples are included, H_- denote the sub-region where the insertion depths of all the low stiffness samples are included, respectively. Then H_A is the overlap of H_+ and H_-, H_{I+} is the remained region of H_+ after removing H_A, and H_{I-} is the remained region of H_- after removing H_A. Therefore, the stiffness classification in terms of insertion depth is given by

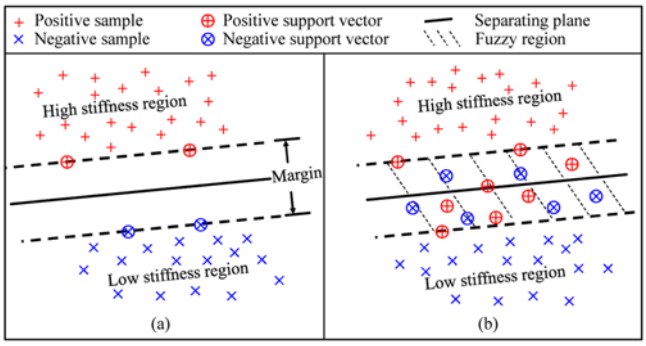

Fig. 4 Illustration of classification and fuzzy region based on SVM, (a) hard margin case, (b) soft margin case

$$K(\boldsymbol{f}_r, h) = \begin{cases} k_+, & h \in H_{I+} \\ k_-, & h \in H_{I-} \end{cases} \tag{9}$$

If the insertion depth belongs to H_A, the data samples are further classified according to the distribution of $\boldsymbol{f}_r$. The SVM method is adopted to learn an optimal plane $\boldsymbol{w}\cdot\boldsymbol{f}_r + b = 0$ that separates the classes with maximum margins.[21] The geometric margin $\tilde{r}$ indicates the separation gap width between the two classes, which is given by

$$\tilde{r} = \min_i \frac{y_i(\boldsymbol{w}\cdot\boldsymbol{f}_{ri} + b)}{\|\boldsymbol{w}\|} \tag{10}$$

where i = 1, 2, …, N_t and N_t is the number of the data samples for model training. Setting $\min_i[y_i(\boldsymbol{w}\cdot\boldsymbol{f}_{ri} + b)] = 1 - \xi_i$, the maximization of $\tilde{r}$ is converted to a convex optimization problem,

$$\min_{\boldsymbol{w},b} \frac{\|\boldsymbol{w}\|^2}{2} + c\sum_{i=1}^{m}\xi_i, \quad \text{s.t.} \begin{cases} y_i(\boldsymbol{w}\cdot\boldsymbol{f}_{ri} + b) \ge 1 - \xi_i, \\ \xi_i \ge 0, \end{cases} \tag{11}$$

where ξ_i is a non-negative slack variable, and c is a penalty parameter. The optimal plane satisfying Eq. (11) can be solved based on Lagrangian theory and the sequential minimal optimization (SMO) algorithm.

In the case where two classes are linearly separable, as shown in Fig. 4(a), we use the hard-margin SVM with $\xi_i \equiv 0$. If the two classes' boundaries overlap, as shown in Fig. 4(b), we use the soft-margin SVM that allows $\xi_i \ge 0$ but uses a penalty term to minimize x_i. The *fuzzy region* is defined as the overlap between two classes' boundaries. Let $\boldsymbol{s}_j$ (j = 1, 2, …, N_s) denote the support vectors, which lie on the classes' boundaries. The fuzzy region is expressed as $\{\boldsymbol{f}_r \mid d_- < \boldsymbol{w}\cdot\boldsymbol{f}_r + b < d_+\}$, where

$$\begin{cases} d_+ = \max_j(\boldsymbol{w}\cdot\boldsymbol{s}_j + b) \\ d_- = \min_j(\boldsymbol{w}\cdot\boldsymbol{s}_j + b) \end{cases} \tag{12}$$

If a new sample is in the fuzzy region, the classifier fails to give a confident identification of stiffness. Therefore, the new samples

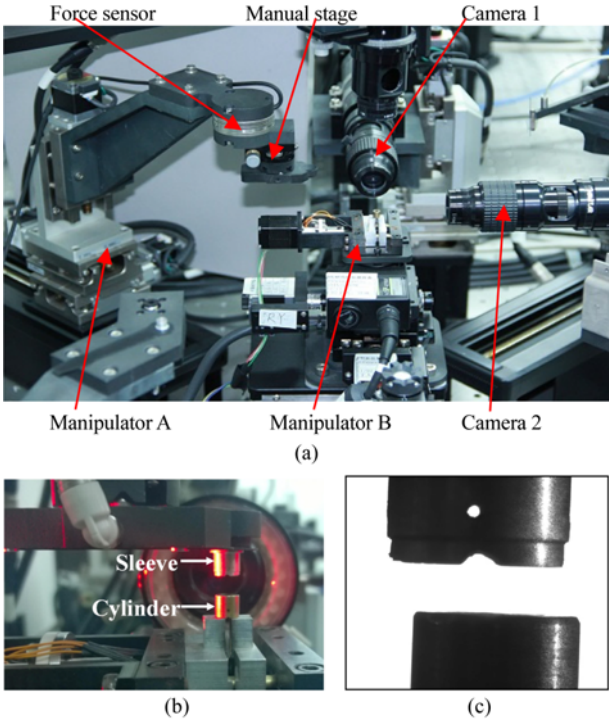

Fig. 5 Experiment system: (a) precision assembly platform, (b) sleeve and cylinder, (c) images of two components

Table 1 Measurement results of translation directions

$\boldsymbol{v}$ (μm)	$\boldsymbol{v}'$	e_θ (°)
$[0,0,-500]^T$	$[-0.00038576,0.00038455,-0.99999985]^T$	0.03
$[20,-10,-500]^T$	$[0.03924673,-0.018246652,-0.999062938]^T$	0.11
$[-50,80,-500]^T$	$[-0.09818913,0.15440040,-0.983117192]^T$	0.16

distributed in the fuzzy region are categorized into the higher stiffness class so that the controller will adjust to a more compliant state. Finally, the stiffness based on the classification is given as,

$$K(\boldsymbol{f}_r,h)=\begin{cases}k_+, & h\in H_{I+} \text{ or } (h\in H_A \,\&\, \boldsymbol{w}\cdot\boldsymbol{f}_r+b\geq d_-)\\ k_-, & h\in H_{I-} \text{ or } (h\in H_A \,\&\, \boldsymbol{w}\cdot\boldsymbol{f}_r+b< d_-)\end{cases} \quad (13)$$

5. Experiments and Results

5.1 Experiment system

The precision assembly system was built based on the design scheme in Section 2, as shown in Fig. 5(a). The manipulator A was constructed with three Sugura KWG06030G motorized stages whose positioning resolution was 1 μm. The vertical motion of the manipulator B was realized with the Micos ES-100 vertical stage, and its resolution was 1 μm. The 6D force/torque sensor ATI Nano-43 provided the 1/128 N force resolution with the 2 kHz sampling frequency. The raw signal of the force sensor was filtered by a Butterworth low-pass filter whose passband frequency and stopband frequency were 20 Hz and 100 Hz, respectively.

The components and their images are shown in Figs. 5(b) and 5(c). The cylinder's size was 50 μm in thickness, 4 mm in height and 5 mm in outer radius. The interference between the cylinder's outer surface and the sleeve's inner wall was about 10 μm. Both components were chamfered at the ends. The non-damage range of radial contact force was 0~300 mN.

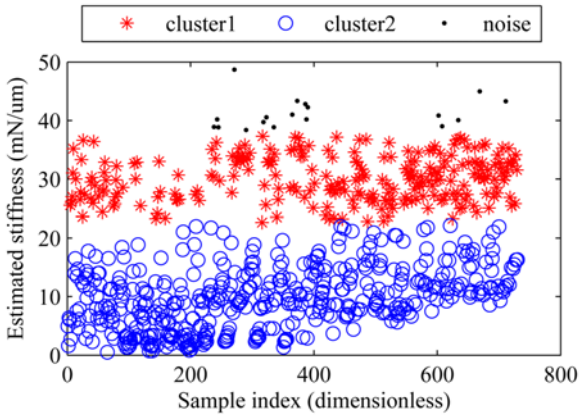

Fig. 6 Clustering result based on DBSCAN

5.2 Attitude measurement based on microscopic vision

To examine the accuracy of the attitude measurement method based on microscopic vision, a metal ball was attached on the manipulator A's end-effector. The manipulator A translated actively by $\boldsymbol{v}=[\Delta x, \Delta y, \Delta z]^T$ μm, and the ball center's translation formed a vector $\boldsymbol{v}$ in {M}. The position changes of the ball image's center in the camera X and Y were obtained as $\boldsymbol{l}_1$ and $\boldsymbol{l}_2$, respectively, using image processing techniques. The normalized direction vector of the ball translation was measured as $\boldsymbol{v}'$ using the vision system, and the angle error between the measured translation direction $\boldsymbol{v}'$ and the exact translation vector $\boldsymbol{v}$ was labeled as e_θ. The results of three attitude measurements were given in Table 1, in which the maximum angle error was 0.16° when the translation direction's inclined angle was within 10°. Therefore, the proposed attitude measurement method provided the sufficient accuracy for force decomposition.

5.3 Anisotropic stiffness learning results

An experience data set with 730 samples was obtained from the past twenty assembly processes, utilizing the radial force control with constant gain. The DBSCAN algorithm's parameters Eps and MinPts were set as 0.5 and 20, respectively. Two clusters 1 and 2 were discovered, whose stiffness averages were 11.2 mN/μm and 30.1mN/μm, respectively. The visualized result is shown in Fig. 6.

The insertion depth region [0,4] mm was divided into sub-regions H_A = [2.2,4] mm, and H_{I-} = [0, 2.2) mm. The samples' distribution in the f_x-f_y-h space is displayed in Fig. 7. Since the angle between the sleeve's axis and the force sensor's z axis was small, the force variations of the samples were mainly caused by f_x and f_y. Therefore, the sample set $\{[f_{xi}, f_{yi}]^T \mid h_i \in H_A\}$ was used as the SVM algorithm's training set.

The penalty parameter utilized in soft margin SVM was set as 10. The learned results were as follows. The separating plane's parameters were $\boldsymbol{w}'$ = [-0.456553, 0.889696, 0]^T and b' = 0.618107. The fuzzy region's parameters were d'_+ = 15.688 and d'_- = -18.184. The samples' distribution in the f_x-f_y space and the learned separating line is shown in Fig. 8.

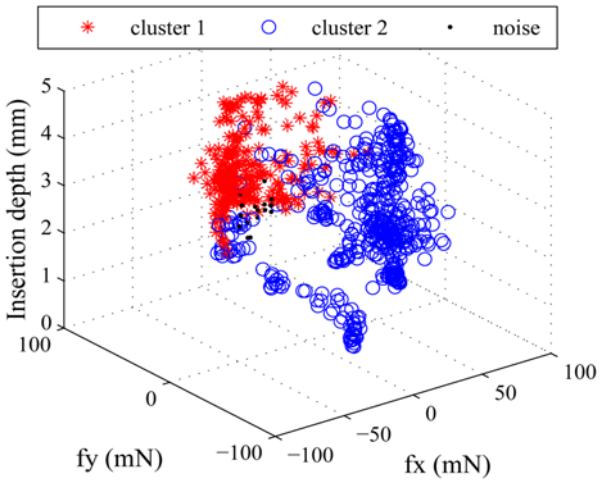

Fig. 7 Samples' distribution in the f_x-f_y-h space

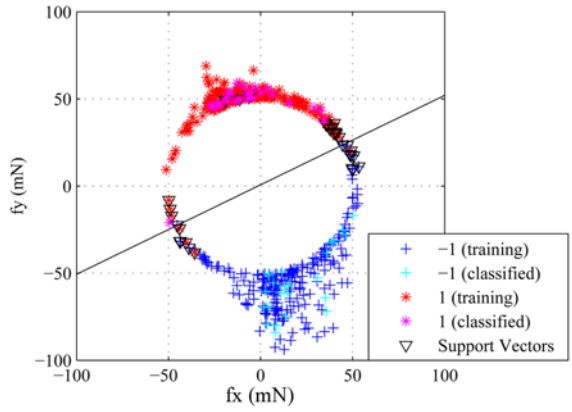

Fig. 8 Samples' distribution in the f_x-f_y space, and the separating line solved by the soft margin SVM

5.4 Anisotropic stiffness radial force control

In this experiment, the learning results of anisotropic stiffness characteristics were used to configure the anisotropic stiffness radial force control method. The incremental controller's gain λ was adjusted according to the predicted stiffness $K(\boldsymbol{f}_r,h)$, which yielded

$$\lambda = \begin{cases} 0.09, & h \in [0,2.2) \text{ or } (h \in [2.2,5] \,\&\, \boldsymbol{w}' \cdot \boldsymbol{f}_r + b' < -18.184) \\ 0.03, & h \in [2.2,5] \,\&\, \boldsymbol{w}' \cdot \boldsymbol{f}_r + b' \geq -18.184 \end{cases}$$

To compare the performances of the traditional method and the proposed method, five groups of assembly experiments were carried out under different component-attitude settings. The component-attitude setting means manually adjusting the sleeve to a specified attitude before assembly. Here the sleeve's attitude was indicated by θ_1 and θ_2, which were the incline angles of the sleeve axis in the images of the camera 1 and 2, respectively. Because component's attitude highly influenced the contact directions during insertion, insertion under various attitudes could show the control method's adaptability to stiffness anisotropy. In the group A, the component-attitude setting was $\theta_1 = 0°$ and $\theta_2 = 0°$. In the group B, $\theta_1 = -1°$, $\theta_2 = 0°$. In the group C, $\theta_1 = 1°$, $\theta_2 = 0°$. In the group D, $\theta_1 = 0°$, $\theta_2 = -1°$. In the group E, $\theta_1 = 0°$, $\theta_2 = 1°$. In each group, the assembly experiments were conducted under the same component-attitude setting using the three control methods: the proposed anisotropic stiffness radial force control, the traditional radial force control with the constant gain $\lambda = 0.03$ and the traditional radial force control with the constant gain $\lambda = 0.09$, respectively. The same dead zone threshold $\tau = 50$ mN was applied. During each insertion process, the measured radial contact forces were recorded at the frequency of 100 Hz.

Table 2 Comparison experimental results

Method	Group No.	Time cost (s)	Compliant motion times	Peak force (mN)
Anisotropic stiffness radial force control	A	23.17	13	76.4
	B	28.27	26	88.9
	C	27.77	28	86.3
	D	21.75	10	70.7
	E	32.58	37	68.5
Radial force control with the constant gain $\lambda = 0.03$	A	30.35	32	80.2
	B	46.73	75	97.9
	C	28.16	28	70.3
	D	27.40	27	82.4
	E	48.87	82	71.8
Radial force control with the constant gain $\lambda = 0.09$	A	29.82	32	81.2
	B	34.85	42	91.0
	C	54.71	91	124.1
	D	40.55	57	92.7
	E	34.59	42	101.3

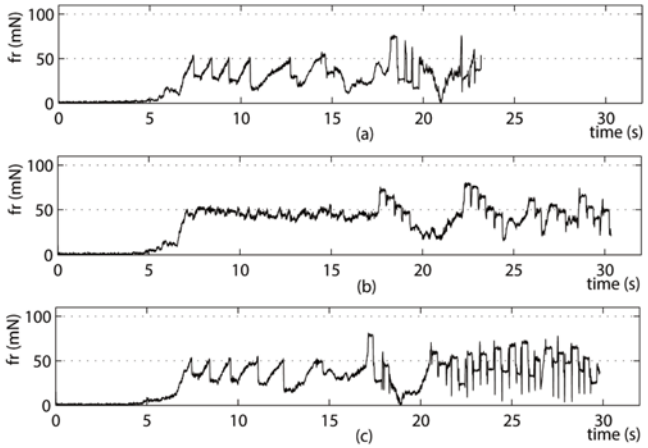

Fig. 9 The radial force magnitude's curves of experiment group A using different methods, (a) anisotropic stiffness radial force control, (b) radial force control with the constant gain $\lambda = 0.03$, (c) radial force control with the constant gain $\lambda = 0.09$

Table 2 exhibits the time costs, compliant motion times and peak radial contact forces during the insertions of the five groups of experiments. As a representative demonstration, the curves of the radial contact force magnitude in the group A are shown in Fig. 9. Although the traditional method could maintain the radial contact force under 130 mN, its performance became worse under some component attitudes, resulting in longer cost time, more frequent compliant motions, and larger peak forces. The reason was that the constant-gain controllers could not adapt to the anisotropic stiffness. In comparison, the proposed

method had the better performances under the different component attitudes. Due to the gain adjustment according to anisotropic stiffness, the frequent compliant motions and large force peaks were avoided. The average insertion time cost was 25.71 s, which was 31% less than that of the traditional method. The maximum radial contact force was 88.9 mN, which was 28% less than that of the traditional method.

In this precision assembly system, the stiffness anisotropy resulted from the manual regulation stage Sigma Koki KKD-25C, which was fixed between the wrist and the gripper of the manipulator A. The manual regulation stage owns the advantages of lightweight and small size comparing to the motorized stage, and is widely used in precision assembly systems whose operation space is small and shared by multi manipulators. However, it was composed by screws, springs and hinges, so that its structure was not symmetrical in all directions. Therefore, the stiffness in radial contact appeared the anisotropic characteristics.

The components were chamfered at the end, so that the two components had a small clearance and their contact was not permanent at the beginning of an insertion. As the insertion depth increased, the clearance decreased to zero, and the two components started to have a permanent interference contact and the contact area increased. As a result, the insertion depth influenced the stiffness, and the estimated stiffness was low when the insertion depth was small.

6. Conclusions and Future Works

In this paper, an active radial compliance method with anisotropic stiffness learning is proposed. The anisotropic stiffness radial force control method, which is based on the explicit force control and the microscopic vision measurement, is able to limit the radial contact force within the desired range. With anisotropic stiffness learning, the anisotropic stiffness characteristics of the mechanical system are obtained from experience data, and the learning results are used to configure the anisotropic stiffness radial force control. Experimental results show that the proposed method leads to accurate and efficient insertion in the cylinder-sleeve assembly.

If more than two clusters are discovered in anisotropic stiffness learning, the stiffness identification will become a multiclass classification problem, which can also be well solved by support vector machines.[22] Therefore, the proposed method can be extended to the cases where multiple clusters exist. Future research will focus on the active compliance method that can deal with small misalignment of components' attitudes.

ACKNOWLEDGEMENT

This work is supported in part by the National Natural Science Foundation of China under grant 61421004, 61227804, 61673382, 61305115, and 61503378.

REFERENCES

1. Wang, W., Loh, R. N. K., and Gu, E. Y., "Passive Compliance Versus Active Compliance in Robot-Based Automated Assembly Systems," Industrial Robot: An International Journal, Vol. 25, No. 1, pp. 48-57, 1998.
2. Volpe, R. and Khosla, P., "A Theoretical and Experimental Investigation of Explicit Force Control Strategies for Manipulators," IEEE Transactions on Automatic Control, Vol. 38, No. 11, pp. 1634-1650, 1993.
3. Sariyildiz, E. and Ohnishi, K., "On the Explicit Robust Force Control via Disturbance Observer," IEEE Transactions on Industrial Electronics, Vol. 62, No. 3, pp. 1581-1589, 2015.
4. Jung, S., Hsia, T. C., and Bonitz, R. G., "Force Tracking Impedance Control of Robot Manipulators under Unknown Environment," IEEE Transactions on Control Systems Technology, Vol. 12, No. 3, pp. 474-483, 2004.
5. Xiao, D., Ghosh, B. K., Xi, N., and Tarn, T. J., "Sensor-Based Hybrid Position/Force Control of a Robot Manipulator in an Uncalibrated Environment," IEEE Transactions on Control Systems Technology, Vol. 8, No. 4, pp. 635-645, 2000.
6. Kumar, N., Panwar, V., Sukavanam, N., Sharma, S. P., and Borm, J.-H., "Neural Network Based Hybrid Force/Position Control for Robot Manipulators," Int. J. Precis. Eng. Manuf., Vol. 12, No. 3, pp. 419-426, 2011.
7. Xie, Y., Sun, D., Liu, C., and Cheng, S. H., "An Adaptive Impedance Force Control Approach for Robotic Cell Microinjection," Proc. of IEEE/RSJ International Conference on Intelligent Robots and Systems, pp. 907-912, 2008.
8. Yamamoto, H. and Sano, T., "Study of Micromanipulation Using Stereoscopic Microscope," IEEE Transactions on Instrumentation and Measurement, Vol. 51, No. 2, pp. 182-187, 2002.
9. Yang, G., Gaines, J. A., and Nelson, B. J., "A Supervisory Wafer-Level 3D Microassembly System for Hybrid MEMS Fabrication," Journal of Intelligent and Robotic Systems, Vol. 37, No. 1, pp. 43-68, 2003.
10. Dechev, N., Cleghorn, W. L., and Mills, J. K., "Microassembly of 3-D Microstructures Using a Compliant, Passive Microgripper," Journal of Microelectromechanical Systems, Vol. 13, No. 2, pp. 176-189, 2004.
11. Borchert, G., Burisch, A., and Raatz, A., "APIS - A Miniaturized Robot for Precision Assembly with Low-Cost Piezoelectric Motors," Int. J. Precis. Eng. Manuf., Vol. 12, No. 4, pp. 629-634, 2011.
12. Xu, Q., "Precision Position/Force Interaction Control of a Piezoelectric Multimorph Microgripper for Microassembly," IEEE Transactions on Automation Science and Engineering, Vol. 10, No. 3, pp. 503-514, 2013.
13. Komati, B., Rabenorosoa, K., Clévy, C., and Lutz, P., "Automated Guiding Task of a Flexible Micropart Using a Two-Sensing-Finger Microgripper," IEEE Transactions on Automation Science and Engineering, Vol. 10, No. 3, pp. 515-524, 2013.

14. Liu, S., Xu, D., Zhang, D., and Zhang, Z., "High Precision Automatic Assembly Based on Microscopic Vision and Force Information," IEEE Transactions on Automation Science and Engineering, Vol. 13, No. 1, pp. 382-393, 2016.

15. Xing, D., Liu, F., Qin, F., and Xu, D., "Coordinated Insertion Control for Inclined Precision Assembly," IEEE Transactions on Industrial Electronics, Vol. 63, No. 5, pp. 2990-2999, 2016.

16. Li, Y. and Ge, S. S., "Impedance Learning for Robots Interacting with Unknown Environments," IEEE Transactions on Control Systems Technology, Vol. 22, No. 4, pp. 1422-1432, 2014.

17. Jaura, A. K., Krouglicof, N., and Osman, M., "Using a Logic Branching Weighted Algorithm to Train Robots for Splined Shaft-Hole Assembly," IEEE Transactions on Systems, Man, and Cybernetics-Part A: Systems and Humans, Vol. 29, No. 3, pp. 277-283, 1999.

18. Li, J., Li, Z., and Chen, J., "Microassembly Path Planning Using Reinforcement Learning for Improving Positioning Accuracy of a 1 cm^3 Omni-Directional Mobile Microrobot," Applied Intelligence, Vol. 34, No. 2, pp. 211-225, 2011.

19. Forsyth, D. A. and Ponce, J., "Optimization Techniques," in: Computer Vision: A Modern Approach, 2nd Ed., Forsyth, D. A., Ponce, J., (Eds.), Prentice Hall, pp. 663-682, 2012.

20. Ester, M., Kriegel, H.-P., Sander, J., and Xu, X., "A Density-Based Algorithm for Discovering Clusters in Large Spatial Databases with Noise," Proc. of the 2nd International Conference on Knowledge Discovery and Data Mining, pp. 226-231, 1996.

21. Cristianini, N. and Shawe-Taylor, J., "Support Vector Machines," in: An Introduction to Support Vector Machines and other Kernel-Based Learning Methods, Cristianini, N., Shawe-Taylor, J., (Eds.), Cambridge University Press, Chap. 6, 2000.

22. Hsu, C.-W. and Lin, C.-J., "A Comparison of Methods for Multiclass Support Vector Machines," IEEE Transactions on Neural Networks, Vol. 13, No. 2, pp. 415-425, 2002.